

The Hadronic Contribution to the Muon Anomalous Magnetic Moment and to the Running Electromagnetic Fine Structure Constant at M_Z — Overview and Latest Results

Andreas Hoecker

CERN, CH-1211, Geneva 23, Switzerland

(Dated: September 24, 2018)

Quantum loops induce an anomaly, a_μ , in the magnetic moment of the muon that can be accurately measured. Its Standard Model prediction is limited in precision by contributions from hadronic vacuum polarisation of the photon. The dominant lowest-order hadronic term can be calculated with a combination of experimental cross section data, involving e^+e^- annihilation to hadrons, and perturbative QCD. These are used to evaluate an energy-squared dispersion integral that strongly emphasises low photon virtualities. The dominant contribution to the integral stems from the two-pion channel that can be measured both in e^+e^- annihilation and in τ decays. The corresponding e^+e^- and τ -based predictions of a_μ exhibit deviations by, respectively, 3.6σ and 2.4σ from experiment, leaving room for a possible interpretation in terms of new physics. This talk reviews the status of the Standard Model prediction with emphasis on the lowest-order hadronic contribution. Also given is the latest result for the running electromagnetic fine structure constant at the Z -mass pole, whose precision is limited by hadronic vacuum polarisation contributions, determined in a way similar to those of the magnetic anomaly.

I. INTRODUCTION

The Dirac equation predicts a muon magnetic moment, $\mathbf{M} = g_\mu \frac{e}{2m_\mu} \mathbf{S}$, with gyromagnetic ratio $g_\mu = 2$. Quantum loop effects lead to a small calculable deviation from $g_\mu = 2$, parametrised by the anomalous magnetic moment

$$a_\mu \equiv \frac{g_\mu - 2}{2}. \quad (1)$$

That quantity can be accurately measured and, within the Standard Model (SM) framework, precisely predicted. Hence, comparison of experiment and theory tests the SM at its quantum loop level. A deviation in a_μ^{exp} from the SM expectation would signal effects of new physics, with current sensitivity reaching up to mass scales of $\mathcal{O}(\text{TeV})$ [1, 2].¹ For recent and very thorough muon $g - 2$ reviews, see Refs. [3, 4].

The E821 experiment at Brookhaven National Lab (BNL) studied the spin precession of μ^+ and μ^- in a constant external magnetic field as they circulated in a confining storage ring. The muon momentum of 3.1 GeV was chosen such that the difference between precession and cyclotron frequency, ω_a , is approximately independent of the electrical quadrupole field, required for the vertical focusing of the muons. This is the case for a Lorentz factor of $\gamma_\mu = \sqrt{1 + 1/a_\mu} \approx 29.3$. The muon

anomalous magnetic moment is then directly given by $a_\mu = \omega_a m_\mu c / (eB)$. The magnetic field strength and homogeneity was precisely measured from NMR probes frequently pulled with a trolley on rails through the ring, and ω_a was obtained from a fit to the decay electron (or positron) counting rates in scintillators installed along the cyclotron. The results were obtained by independently blinding B and ω_a until all systematic studies were terminated to satisfaction. The final published results read [6]²

$$a_{\mu^+}^{\text{exp}} = (11\,659\,204 \pm 6 \pm 5) \times 10^{-10}, \quad (2)$$

$$a_{\mu^-}^{\text{exp}} = (11\,659\,215 \pm 8 \pm 3) \times 10^{-10}, \quad (3)$$

where the first errors are statistical and the second systematic. Assuming CPT invariance and taking into account correlations between systematic errors, one finds for their average [6]

$$a_\mu^{\text{exp}} = (11\,659\,208.9 \pm 5.4 \pm 3.3) \times 10^{-10}. \quad (4)$$

These results represent about a factor of 14 improvement over the classic CERN experiments of the 1970's [8].

The SM prediction for a_μ^{SM} is conveniently separated into three parts (see Fig. 1 for representative Feynman diagrams)

$$a_\mu^{\text{SM}} = a_\mu^{\text{QED}} + a_\mu^{\text{EW}} + a_\mu^{\text{had}}. \quad (5)$$

¹ Although the corresponding electron anomalous magnetic moment has been measured approximately 800 times more accurately than the muon one, its sensitivity to new physics is expected to be about 50 times lower, owing to the quadratic lepton-mass dependence of the virtual contribution from new, heavy particles.

² The original results reported by the experiment have been updated in Eqs. (2)–(4) to the newest value for the absolute muon-to-proton magnetic ratio $\lambda = 3.183345137 \pm 85$ [5]. The change induced in a_μ^{exp} with respect to the value of $\lambda = 3.18334539 \pm 10$ used in Ref. [6] amounts to $+0.92 \times 10^{-10}$ [7].

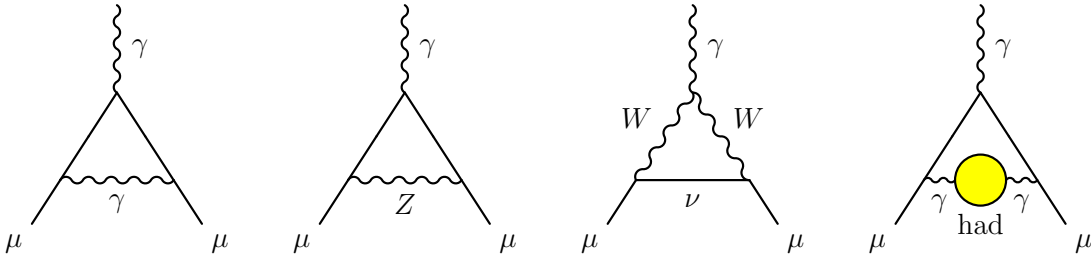


FIG. 1: Representative diagrams contributing to a_μ^{SM} . From left to right: first order QED (Schwinger term), lowest-order weak, lowest-order hadronic.

The QED part includes all photonic and leptonic (e, μ, τ) loops starting with the classic $\alpha/2\pi$ Schwinger contribution. It has been computed through 4 loops and estimated at the 5-loop level [9]

$$a_\mu^{\text{QED}} = \frac{\alpha}{2\pi} + 0.765857410(27) \left(\frac{\alpha}{\pi}\right)^2 + 24.05050964(43) \left(\frac{\alpha}{\pi}\right)^3 + 130.8055(80) \left(\frac{\alpha}{\pi}\right)^4 + 663(20) \left(\frac{\alpha}{\pi}\right)^5 + \dots, \quad (6)$$

where the errors in each term are given in parentheses. Employing $\alpha^{-1} = 137.035999084(51)$, determined [9, 10] from the electron a_e measurement, leads to

$$a_\mu^{\text{QED}} = (116\,584\,718.09 \pm 0.15) \times 10^{-11}, \quad (7)$$

where the error account for the uncertainties in the coefficients (6) and in α .

Loop contributions involving heavy W^\pm, Z or Higgs particles are collectively labelled as a_μ^{EW} . They are suppressed by at least a factor of $\frac{\alpha}{\pi} \frac{m_\mu^2}{m_W^2} \simeq 4 \times 10^{-9}$. At 1-loop order one finds [11]

$$a_\mu^{\text{EW}}[1\text{-loop}] = \frac{G_\mu m_\mu^2}{8\sqrt{2}\pi^2} \left[\frac{5}{3} + \frac{1}{3} (1 - 4\sin^2\theta_W)^2 + \mathcal{O}\left(\frac{m_\mu^2}{M_W^2}\right) + \mathcal{O}\left(\frac{m_\mu^2}{m_H^2}\right) \right], \quad (8)$$

$$= 194.8 \times 10^{-11},$$

for $\sin^2\theta_W \equiv 1 - M_W^2/M_Z^2 \simeq 0.223$, and where $G_\mu \simeq 1.166 \times 10^{-5} \text{ GeV}^{-2}$ is the Fermi coupling constant. Two-loop corrections are relatively large and negative [12]

$$a_\mu^{\text{EW}}[2\text{-loop}] = (-40.7 \pm 1.0 \pm 1.8) \times 10^{-11}, \quad (9)$$

where the errors stem from quark triangle loops and the assumed Higgs mass range between 100 and 500 GeV. The 3-loop leading logarithms are negligible [12, 15], $\mathcal{O}(10^{-12})$, implying in total

$$a_\mu^{\text{EW}} = (154 \pm 1 \pm 2) \times 10^{-11}. \quad (10)$$

Hadronic (quark and gluon) loop contributions to a_μ^{SM}

give rise to its main uncertainty. At present, those effects are not calculable from first principles, but such an approach, at least partially, may become possible as lattice QCD matures. Instead, one currently relies on a dispersion relation approach to evaluate the dominant lowest-order $\mathcal{O}(\alpha^2)$ hadronic vacuum polarisation contribution $a_\mu^{\text{had,LO}}$ from corresponding cross section measurements or, where applicable, from perturbative QCD [16]

$$a_\mu^{\text{had,LO}} = \frac{1}{3} \left(\frac{\alpha}{\pi}\right)^2 \int_{m_{\pi^0\gamma}^2}^{\infty} ds \frac{K(s)}{s} R^{(0)}(s), \quad (11)$$

where $K(s)$ is a QED kernel function [17], and where $R^{(0)}(s)$ denotes the ratio of the bare³ cross section for e^+e^- annihilation into hadrons to the pointlike muon-pair cross section at centre-of-mass energy \sqrt{s} . The function $K(s) \sim 1/s$ in Eq. (11) gives a strong weight to the low-energy part of the integral so that $a_\mu^{\text{had,LO}}$ is dominated by the contribution from the $\rho(770) \rightarrow \pi\pi$ resonance. Equation (11) is solved by using sums of exclusive cross section data at low centre-of-mass energies (often chosen to be below 1.8 GeV), inclusive hadronic cross section data in the $c\bar{c}$ threshold region, and perturbative QCD elsewhere.

A huge effort over 20 years and more by experimentalists and theorists went into the determination of the lowest-order hadronic contribution. The most significant improvements came from the experimental side with the availability of more accurate e^+e^- cross section data from Novosibirsk, and by exploiting the high statistics data samples of the B and Φ factories using the technique of radiative return. Using isospin symmetry, precise hadronic τ decay data could also be used to complement the e^+e^- data. The understanding that perturbative QCD works seamlessly down to unexpectedly low energy scales, led to more extensive use of theory to replace less precise data.

³ The bare cross section is defined as the measured cross section corrected for initial-state radiation, electron-vertex loop contributions and vacuum-polarisation effects in the photon propagator. QED effects in the hadron vertex and final state, as photon radiation, are included, i.e., not corrected.

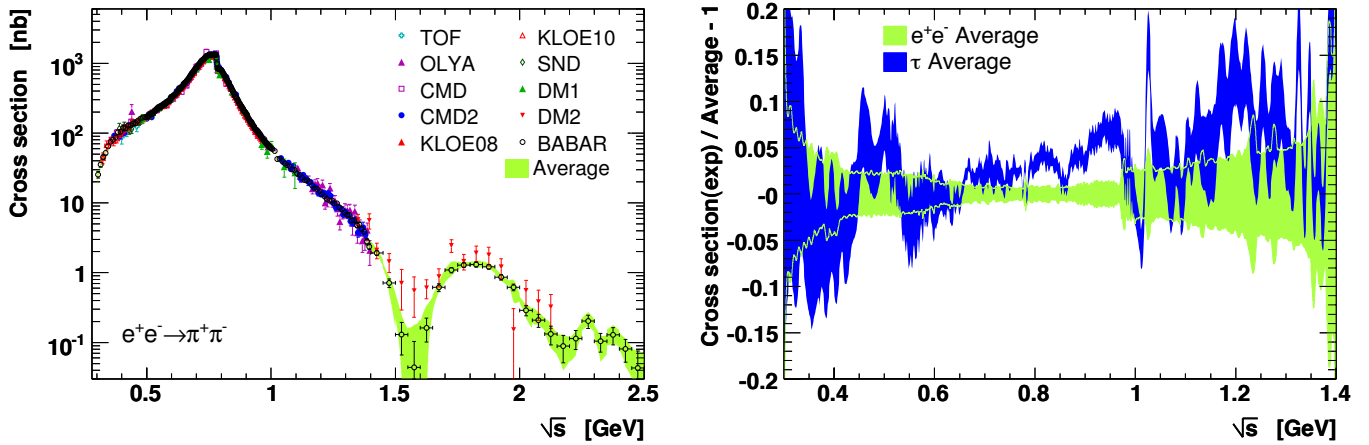


FIG. 2: Left panel: cross section of $e^+e^- \rightarrow \pi^+\pi^-$ versus centre-of-mass energy for different energy ranges (see [18] for references). The error bars show statistical and systematic errors added in quadrature. The light shaded (green) band indicates the average within 1σ errors. Right panel: relative difference between the average $\tau^- \rightarrow \pi^- \pi^0 \nu_\tau$ and $e^+e^- \rightarrow \pi^+\pi^-$ cross sections. The individual measurements show agreement between Belle/CLEO (τ) and BABAR (e^+e^-), but discrepancies between τ and KLOE data.

The analysis of the hadronic contribution reported here has been published [18] after the conference. It includes new $\pi^+\pi^-$ cross-section data from KLOE, all available multi-hadron data from BABAR, a reestimation of missing low-energy contributions using results on cross sections and process dynamics from BABAR, a reevaluation of all experimental contributions using newly developed software, and a reanalysis of inter-experiment and inter-channel correlations, and finally a reevaluation of the continuum contributions from perturbative QCD at four loops.

II. NEW HADRONIC CROSS SECTION DATA

The KLOE Collaboration has published new $\pi^+\pi^-\gamma$ cross section data with $\pi^+\pi^-$ invariant mass-squared between 0.1 and 0.85 GeV^2 [19]. The radiative photon in this analysis is required to be detected in the electromagnetic calorimeter, which reduces the selected data sample to events with large photon scattering angle. The new data are found to be in agreement with, but less precise than previously published data using small angle photon scattering [20]. They exhibit a discrepancy, on the ρ resonance peak and above, with other $\pi^+\pi^-$ data, in particular those from BABAR, obtained with the use of the same ISR technique [21], and with data from $\tau^- \rightarrow \pi^- \pi^0 \nu_\tau$ decays [22] (cf. right-hand panel of Fig. 2).

Figure 2 (left) shows the available $e^+e^- \rightarrow \pi^+\pi^-$ cross section measurements in various panels for different centre-of-mass energies (\sqrt{s}). The light shaded (green) band indicates the average within 1σ errors. The deviation between the average and the most precise individual measurements is depicted in Fig. 3. Figure 4 shows the weights versus \sqrt{s} the different experiments obtain in

the locally performed average. BABAR and KLOE dominate the average over the entire energy range. Owing to the sharp radiator function, the available statistics for KLOE increases towards the ϕ mass, hence outperforming BABAR above ~ 0.8 GeV. For example, at 0.9 GeV KLOE's small photon scattering angle data [20] have statistical errors of 0.5%, which is twice smaller than that of BABAR (renormalising BABAR to the 2.75 times larger KLOE bins at that energy). Conversely, at 0.6 GeV the comparison reads 1.2% (KLOE) versus 0.5% (BABAR, again given in KLOE bins which are about 4.2 times larger than for BABAR at that energy). The discrepancy between the BABAR and KLOE data sets above 0.8 GeV causes error rescaling in their average, and hence loss of precision. The group of experiments labelled “other exp” in Fig. 4 corresponds to older data with incomplete radiative corrections. Their weights are small throughout the entire energy domain.

For the analysis in Ref. [18] the contributions from the $\omega(782)$ and $\phi(1020)$ resonances were computed for the first time directly from the corresponding partial measurements in the $\pi^+\pi^-\pi^0$, $\pi^0\gamma$, $\eta\gamma$, K^+K^- , $K_s^0 K_L^0$ channels. Small remaining decay modes were considered separately.

Also included in Ref. [18] are new, preliminary, $e^+e^- \rightarrow \pi^+\pi^- 2\pi^0$ cross section measurements from BABAR [28], which significantly help to constrain a contribution with disparate experimental information.⁴

⁴ The new measurements also improve the conserved vector current (CVC) predictions for the corresponding τ decays with four pions in the final state. Reference [18] finds $\mathcal{B}_{\text{CVC}}(\tau^- \rightarrow \pi^- 3\pi^0 \nu_\tau) = (1.07 \pm 0.06)\%$, to be compared to the world average of the direct measurements $(1.04 \pm 0.07)\%$ [36], and $\mathcal{B}_{\text{CVC}}(\tau^- \rightarrow 2\pi^- \pi^+ \pi^0 \nu_\tau) = (3.79 \pm 0.21)\%$, to be compared to

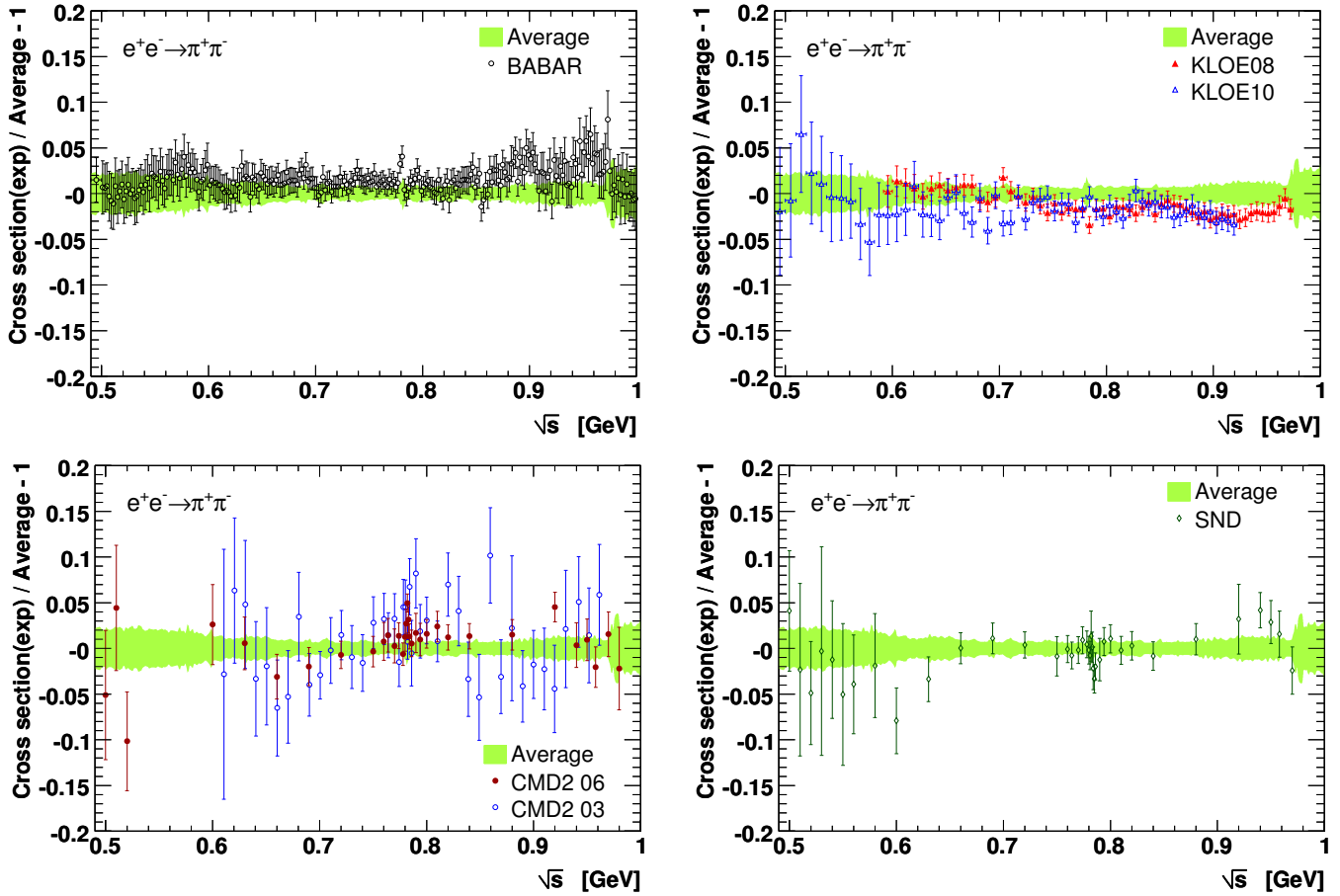


FIG. 3: Comparison between individual $e^+e^- \rightarrow \pi^+\pi^-$ cross section measurements from BABAR [21], KLOE08 [20], KLOE10 [19], CMD2 03 [23], CMD2 06 [24], SND [25], and the average. The error bars show statistical and systematic errors added in quadrature.

Precise BABAR data [29–32] are available for several higher multiplicity modes with and without kaons, which greatly benefit from the excellent particle identification capabilities of the BABAR detector. The new data help to discriminate between older, less precise and sometimes contradicting measurements. Figure 5 shows the cross section measurements and averages for the channels $K^+K^-\pi^+\pi^-$ (upper left), $2\pi^+2\pi^-\pi^0$ (upper right), $3\pi^+3\pi^-$ (lower left), and $2\pi^+2\pi^-\pi^0$ (lower right). The BABAR data supersede much less precise measurements from M3N, DM1 and DM2. In several occurrences, these older measurements overestimate the cross sections in comparison with BABAR, which contributes to the reduction in the size of the present evaluation of hadronic loop effects.

Good agreement is observed among the measurements of the charm resonance region above the opening of the

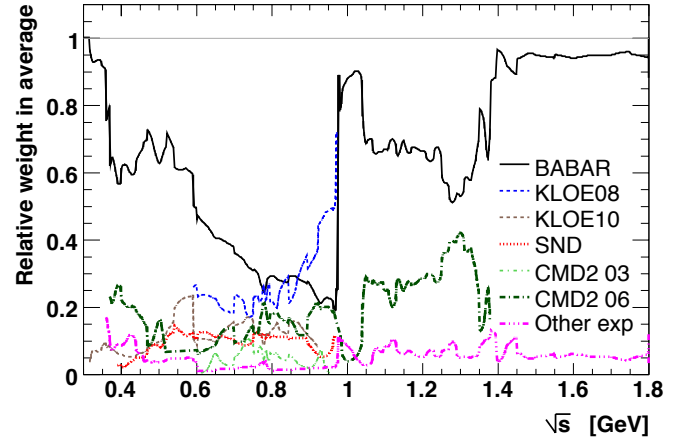


FIG. 4: Relative local averaging weight per experiment versus centre-of-mass energy in $e^+e^- \rightarrow \pi^+\pi^-$.

the direct measurement $(4.48 \pm 0.06)\%$. The deviation between prediction and measurement in the latter channel amounts to 3.2σ , compared to 3.6σ without the BABAR data [33].

$D\bar{D}$ channel [18].

Several five and six-pion modes involving π^0 's, as well as $K\bar{K}[n\pi]$ final states are still unmeasured. Their contributions are estimated from those of known channels

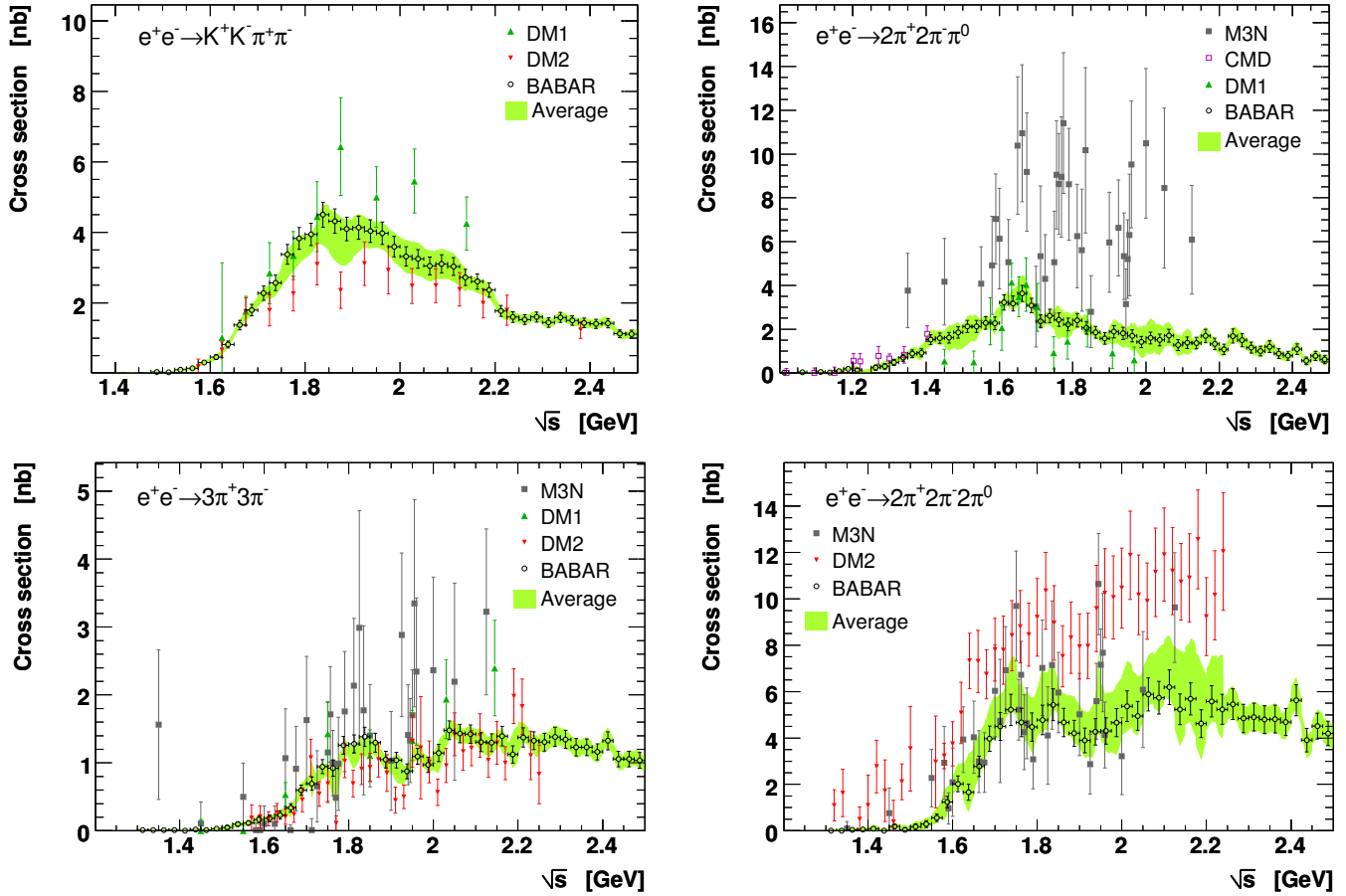


FIG. 5: Cross section data for the final states $K^+K^-\pi^+\pi^-$ (upper left), $2\pi^+2\pi^-\pi^0$ (upper right), $3\pi^+3\pi^-$ (lower left) and $2\pi^+2\pi^-\pi^0$ (lower right). The shaded (green) bands give the averages within 1σ errors, locally rescaled in case of incompatibilities. The BABAR data points are taken from Refs. [27, 29, 30]. The other data points are referenced in [18].

by means of Pais classification of N -pion states with total isospin $I = 0, 1$ [35]. The new BABAR cross section data and results on process dynamics thereby allow more stringent constraints of the unknown contributions than the ones obtained in previous analyses [33, 34]. The re-analysis of the available information led to the following approaches [18]:

- *5-pion channels*: isospin constrains the unmeasured $3\pi^0$ mode by $\sigma(2\pi^+2\pi^-\pi^0) = 2 \cdot \sigma(\pi^+\pi^-3\pi^0)$. The isospin-breaking (IB) $\eta\pi\pi$ contribution is subtracted and treated apart.
- *6-pion channels*: the unknown $\sigma(\pi^+\pi^-4\pi^0)$ is determined from $\sigma(3\pi^+3\pi^-)$ and $\sigma(2\pi^+2\pi^-\pi^0)$, together with an upper limit from $\tau \rightarrow 6\pi\nu$ data on two unconstrained Pais partitions, and using the experimental fact that these modes are dominated by $\omega 3\pi$. IB contributions from $\eta\omega$ are subtracted and treated separately.
- *$KK(n\pi)$ channels*: the missing modes $K_s^0 K_L^0 \pi^0$ and $K_s^0 K^+\pi^-\pi^0$, $K_s^0 K_s^0 \pi^+\pi^-$, $K_s^0 K_L^0 \pi^+\pi^-$ are estimated from $I = 0, 1$ isospin relations using

$K^*(890)K$ dominance, and correcting for small $\phi\pi$ and $KK\rho$ contributions. The $KK\pi\pi\pi$ contribution is determined from the measured $K^+K^-\pi^+\pi^-\pi^0$ using the observed $K^+K^-\omega$ dominance.

- *$\eta 4\pi$ channels*: the total contribution is estimated as twice the measured $\sigma(\eta 2\pi^+2\pi^-)$.

Conservative systematic errors are applied where the dynamical information is incomplete to fully determine all contributing Pais partitions.

III. DATA AVERAGING AND INTEGRATION

For the evaluation in Ref. [18] all experimental cross section data used in the compilation have been evaluated with the software package HVPTools. It replaces linear interpolation between adjacent data points (“trapezoidal rule”) by quadratic interpolation, which is found from pseudo-model analyses, with known truth integrals, to be more accurate. The interpolation functions are locally averaged between experiments, whereby correlations between measurement points of the same experiment and

TABLE I: Contributions to $a_\mu^{\text{had,LO}}$ (middle column) from the individual $\pi^+\pi^-$ cross section measurements by BABAR [21], KLOE [19, 20], CMD2 [23, 24], and SND [25]. Also given are the corresponding CVC predictions of the $\tau \rightarrow \pi^-\pi^0\nu_\tau$ branching fraction (right column), corrected for isospin-breaking effects [22]. Here the first error is experimental and the second estimates the uncertainty in the isospin-breaking corrections. The predictions are to be compared with the world average of the direct branching fraction measurements ($25.51 \pm 0.09\%$ [36]). For each experiment, all available data in the energy range from threshold to 1.8 GeV (m_τ for \mathcal{B}_{CVC}) are used, and the missing part is completed by the combined e^+e^- data. The corresponding (integrand dependent) fractions of the full integrals provided by a given experiment are given in parentheses.

Exp.	$a_\mu^{\text{had,LO}}$ [10^{-10}]	\mathcal{B}_{CVC} [%]
BABAR	514.1 ± 3.8 (1.00)	$25.15 \pm 0.18 \pm 0.22$ (1.00)
KLOE	503.1 ± 7.1 (0.97)	$24.56 \pm 0.26 \pm 0.22$ (0.92)
CMD2	506.6 ± 3.9 (0.89)	$24.96 \pm 0.21 \pm 0.22$ (0.96)
SND	505.1 ± 6.7 (0.94)	$24.82 \pm 0.30 \pm 0.22$ (0.91)

among different experiments due to common systematic errors are fully taken into account. Incompatible measurements lead to error rescaling in the local averages, using the PDG prescription [36].

The errors in the average and in the integration for each channel are obtained from large samples of pseudo Monte Carlo experiments, by fluctuating all data points within errors respecting their correlations. The integrals of the exclusive channels are then summed up, and the error of the sum is obtained by adding quadratically (linearly) all uncorrelated (correlated) errors.

Common sources of systematic errors also occur between measurements of different final state channels and must be taken into account when summing up the exclusive contributions. Such correlations mostly arise from luminosity uncertainties, if the data stem from the same experimental facility, and from radiative corrections. In total eight categories of correlated systematic uncertainties are distinguished [18]. Among those the most significant belong to radiative corrections, which are the same for CMD2 and SND, as well as to luminosity determinations by BABAR, CMD2 and SND (correlated per experiment for different channels, but independent between different experiments).

IV. RESULTS

Table I quotes the specific contributions of the various $e^+e^- \rightarrow \pi^+\pi^-$ cross section measurements to $a_\mu^{\text{had,LO}}$. Also given are the corresponding CVC-based $\tau \rightarrow \pi^-\pi^0\nu_\tau$ branching fraction predictions. The largest (smallest) discrepancy of 2.7σ (1.2σ) between prediction and direct measurement is exhibited by KLOE

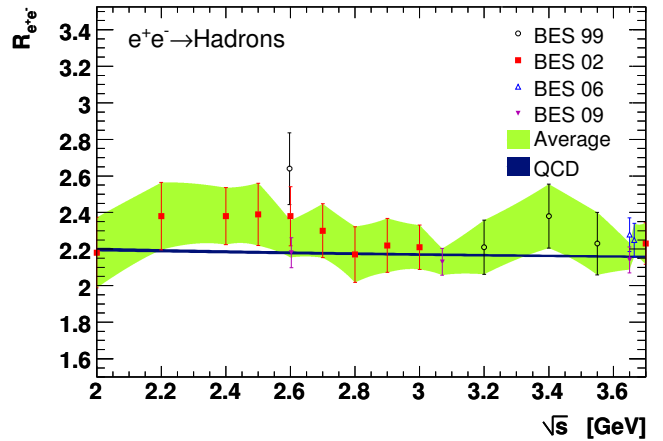


FIG. 6: Inclusive hadronic cross section ratio versus centre-of-mass energy in the continuum region below the $D\bar{D}$ threshold. Shown are bare BES data points [42], with statistical and systematic errors added in quadrature, the data average (shaded band), and the prediction from massive perturbative QCD (solid line—see text).

(BABAR). It is interesting to note that the four $a_\mu^{\text{had,LO}}[\pi^+\pi^-]$ determinations agree within errors (the overall χ^2 of their average amounts to 3.2 for 3 degrees of freedom), whereas significant discrepancies are observed in the corresponding spectral functions [26]. The combined contribution, computed from local averages of the spectral function data, is subjected to local error rescaling in case of incompatibilities.

The contributions of the J/ψ and $\psi(2S)$ resonances are obtained by numerically integrating the corresponding undressed Breit-Wigner lineshapes. The errors in the integrals are dominated by the knowledge of the corresponding bare electronic width $\Gamma_{R \rightarrow ee}^0$.

Sufficiently far from the quark thresholds four-loop [37] perturbative QCD, including $\mathcal{O}(\alpha_s^2)$ quark mass corrections [38], is used to compute the inclusive hadronic cross section versus \sqrt{s} . Non-perturbative contributions at 1.8 GeV were determined from data [39] and found to be small. The error in the perturbative prediction accounts for the uncertainty in α_s ($\alpha_s(M_Z^2) = 0.1193 \pm 0.0028$ from the fit to the Z hadronic width [40] is used), the truncation of the perturbative series (assigning the full four-loop contribution as systematic error), the full difference between fixed-order perturbation theory (FOPT) and, so-called, contour-improved perturbation theory (CIPT) [41], as well as quark mass uncertainties (the values and errors from Ref. [36] are used). The former three errors are taken to be fully correlated between the various energy regions where perturbative QCD is used, whereas the (smaller) quark-mass uncertainties are taken to be uncorrelated. Figure 6 shows the comparison between BES data [42] and the QCD prediction below the $D\bar{D}$ threshold between 2 and 3.7 GeV. Agreement within errors is found. Also for the transition region of 1.75–2.0 GeV, between the sum of exclusive measurements and

QCD, excellent agreement between data and theory is found [18].

A full compilation of all contributions to $a_\mu^{\text{had,LO}}$ is given in Table II of Ref. [18].

Muon magnetic anomaly. Adding all lowest-order hadronic contributions together yields the estimate (this and all following numbers in this and the next paragraph are in units of 10^{-10}) [18]

$$a_\mu^{\text{had,LO}} = 692.3 \pm 1.4 \pm 3.1 \pm 2.4 \pm 0.2 \pm 0.3, \quad (12)$$

where the first error is statistical, the second channel-specific systematic, the third common systematic, correlated between at least two exclusive channels, and the fourth and fifth errors stand for the narrow resonance and QCD uncertainties, respectively. The total error of 4.2 is dominated by experimental systematic uncertainties. The new result is $-3.2 \cdot 10^{-10}$ below the previous one [26]. This shift is composed of -0.7 from the inclusion of the new, large photon angle data from KLOE, $+0.4$ from the use of preliminary BABAR data in the $e^+e^- \rightarrow \pi^+\pi^-\pi^0$ mode, -2.4 from the new high-multiplicity exclusive channels, the re-estimate of the unknown channels, and the new resonance treatment, -0.5 from mainly the four-loop term in the QCD prediction of the hadronic cross section that contributes with a negative sign, as well as smaller other differences. The total error on $a_\mu^{\text{had,LO}}$ is slightly larger than that of Ref. [26] owing to a more conservative evaluation of the inter-channel correlations.

Adding to the result (12) the contributions from higher order hadronic loops, -9.79 ± 0.09 [44], computed using a similar dispersion relation approach, hadronic light-by-light scattering (LBLS), 10.5 ± 2.6 [46], estimated from theoretical model calculations (cf. remark in Footnote 5), as well as QED (7), and electroweak effects (10), one obtains the full SM prediction

$$a_\mu^{\text{SM}} = 11\,659\,180.2 \pm 4.2 \pm 2.6 \pm 0.2 \text{ (4.9}_{\text{tot}}), \quad (13)$$

where the errors have been split into lowest and higher order hadronic, and other contributions, respectively. The result (13) deviates from the experimental average (4) by 28.7 ± 8.0 (3.6σ).⁵

A compilation of recent SM predictions for a_μ compared with the experimental result is given in Fig. 7.

Update of τ -based $g-2$ result. Since the majority of the analysis in the a_μ analysis also affects the τ -based result from Ref. [22], a reevaluation of the corresponding τ -based hadronic contribution has been performed in Ref. [18]. In the τ -based analysis [47], the $\pi^+\pi^-$

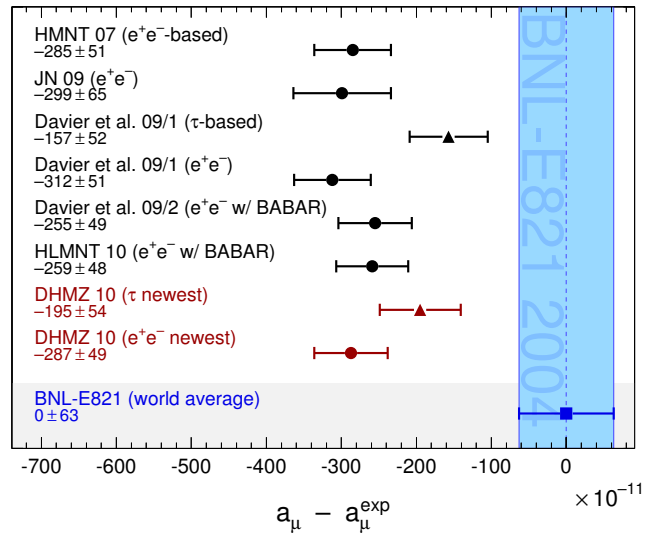


FIG. 7: Compilation of recent results for a_μ^{SM} (in units of 10^{-11}), subtracted by the central value of the experimental average (4). The shaded vertical band indicates the experimental error. The SM predictions are taken from: DHMZ 10 [18], HLMNT (unpublished) [43] (e^+e^- based, including BABAR and KLOE 2010 $\pi^+\pi^-$ data), Davier *et al.* 09/1 [22] (τ -based), Davier *et al.* 09/1 [22] (e^+e^- -based, not including BABAR $\pi^+\pi^-$ data), Davier *et al.* 09/2 [26] (e^+e^- -based including BABAR $\pi^+\pi^-$ data), HMNT 07 [44] and JN 09 [45] (not including BABAR $\pi^+\pi^-$ data).

cross section is entirely replaced by the average, isospin-transformed, and isospin-breaking corrected $\tau \rightarrow \pi^-\pi^0\nu_\tau$ spectral function,⁶ while the four-pion cross sections, obtained from linear combinations of the $\tau^- \rightarrow \pi^-3\pi^0\nu_\tau$ and $\tau^- \rightarrow 2\pi^-\pi^+\pi^0\nu_\tau$ spectral functions, are only evaluated up to 1.5 GeV with the τ data. Due to the lack of statistical precision, the spectrum is completed with the use of e^+e^- data between 1.5 and 1.8 GeV. All the other channels are taken from e^+e^- data. The complete lowest-order τ -based result reads [18]

$$a_\mu^{\text{had,LO}}[\tau] = 701.5 \pm 3.5 \pm 1.9 \pm 2.4 \pm 0.2 \pm 0.3, \quad (14)$$

where the first error is τ experimental, the second estimates the uncertainty in the isospin-breaking corrections, the third is e^+e^- experimental, and the fourth and fifth stand for the narrow resonance and QCD uncertainties, respectively. The τ -based hadronic contribution differs by 9.1 ± 5.0 (1.8σ) from the e^+e^- -based one, and the full τ -based SM prediction $a_\mu^{\text{SM}}[\tau] = 11\,659\,189.4 \pm 5.4$ differs by 19.5 ± 8.3 (2.4σ) from the experimental average. This τ -based result is also included in the compilation of Fig. 7.

⁵ Using alternatively 11.6 ± 4.0 [14] for the light-by-light scattering contribution, increases the error in the SM prediction (13) to 5.8, and reduces the discrepancy with experiment to 3.2σ .

⁶ Using published $\tau \rightarrow \pi^-\pi^0\nu_\tau$ spectral function data from ALEPH [48], Belle [49], CLEO [50] and OPAL [51], and using the world average branching fraction [36] (2009 PDG edition).

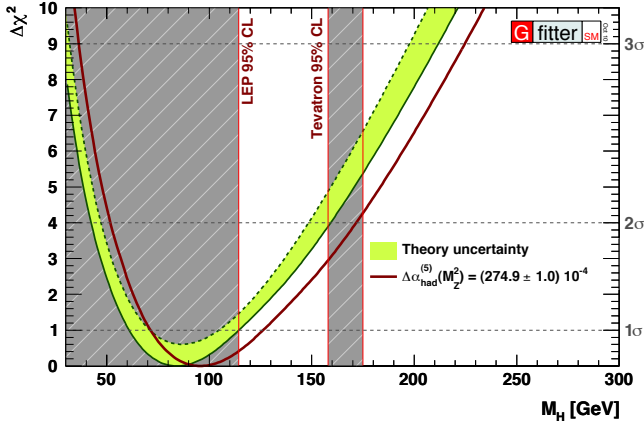


FIG. 8: Standard Gfitter electroweak fit result [40] (green shaded band) and the result obtained for the new evaluation of $\Delta\alpha_{\text{had}}(M_Z^2)$ (red solid curve). Note that the legend displays the corresponding five-quark contribution, $\Delta\alpha_{\text{had}}^{(5)}(M_Z^2)$, where the top term of $-0.72 \cdot 10^{-4}$ is excluded. A shift of +12 GeV in the central value of the Higgs boson is observed.

Running electromagnetic fine structure constant at M_Z^2 . The running electromagnetic fine structure constant, $\alpha(s) = \alpha(0)/(1 - \Delta\alpha_{\text{lep}}(s) - \Delta\alpha_{\text{had}}(s))$, at the scale of the Z mass-squared, $s = M_Z^2$, is an important ingredient of the SM fit to electroweak precision data at the Z pole. Similar to a_μ , the error on the $\alpha(M_Z)$ is dominated by hadronic vacuum polarisation.

The sum of all the hadronic contributions gives for the e^+e^- -based hadronic term in the running of $\alpha(M_Z^2)$

$$\Delta\alpha_{\text{had}}(M_Z^2) = (274.2 \pm 1.0) \cdot 10^{-4}, \quad (15)$$

which is, contrary to the evaluation of $a_\mu^{\text{had,LO}}$, not dominated by the uncertainty in the low-energy data, but by contributions from all energy regions, where both experimental and theoretical errors are of similar magnitude. The corresponding τ -based result reads $\Delta\alpha_{\text{had}}(M_Z^2) = (275.4 \pm 1.1) \cdot 10^{-4}$. As expected, the result (15) is smaller than the most recent (unpublished) value from the HLMNT group [43] $\Delta\alpha_{\text{had}}(M_Z^2) = (275.2 \pm 1.5) \cdot 10^{-4}$. Owing to the use of perturbative QCD between 1.8 and 3.7 GeV, the precision in Eq. (15) is significantly improved compared to the HLMNT result, which relies on experimental data in that domain.⁷

Adding the three-loop leptonic contribution, $\Delta\alpha_{\text{lep}}(M_Z^2) = 314.97686 \cdot 10^{-4}$ [52], with negligible uncertainty, one finds

$$\alpha^{-1}(M_Z^2) = 128.962 \pm 0.014. \quad (16)$$

The running electromagnetic coupling at M_Z enters at various levels the global SM fit to electroweak precision data. It contributes to the radiator functions that modify the vector and axial-vector couplings in the partial Z boson widths to fermions, and also to the SM prediction of the W mass and the effective weak mixing angle. Overall, the fit exhibits a -39% correlation between the Higgs mass (M_H) and $\Delta\alpha_{\text{had}}(M_Z^2)$ [40], so that the decrease in the value (15) and thus in the running electromagnetic coupling strength with respect to earlier evaluations leads to an increase in the best fit value for M_H .⁸ Figure 8 shows the standard Gfitter result (green shaded band) [40], using as hadronic contribution $\Delta\alpha_{\text{had}}(M_Z^2) = (276.8 \pm 2.2) \cdot 10^{-4}$ [44], together with the result obtained by using Eq. (15) (red solid line). The fitted Higgs mass shifts from previously 84_{-23}^{+31} GeV to 96_{-24}^{+30} GeV. The larger error of the latter value, in spite of the improved accuracy in $\Delta\alpha_{\text{had}}(M_Z^2)$, is due to the logarithmic M_H dependence of the fit observables. The new 95% and 99% upper limits on M_H are 170 GeV and 201 GeV, respectively.

V. CONCLUSIONS

Updated Standard Model predictions of the hadronic contributions to the muon anomalous magnetic moment and to the running electromagnetic coupling constant at M_Z^2 have been reported in Ref. [18]. Mainly the reestimation of missing higher multiplicity channels, owing to new results from BABAR, causes a decrease of this contribution with respect to earlier evaluations, which—on one hand—amplifies the discrepancy of the muon $g - 2$ measurement with its prediction to 3.6σ for e^+e^- -based analysis, and to 2.4σ for the τ -based analysis, while—on the other hand—it relaxes the tension between the direct Higgs searches and the electroweak fit by 12 GeV for the Higgs mass.

A thorough reestimation of inter-channel correlations led to a slight increase in the final error of the hadronic contribution to the muon $g - 2$. A better precision is currently constricted by the discrepancy between KLOE and the other experiments, in particular BABAR, in the dominant $\pi^+\pi^-$ mode. This discrepancy is corroborated when comparing e^+e^- and τ data in this mode, where agreement between BABAR and the τ data is observed.

Support for the KLOE results must come from a cross-section measurement involving the ratio of pion-to-muon pairs. Moreover, new $\pi^+\pi^-$ precision data are soon expected from the upgraded VEPP-2000 storage ring at BINP-Novosibirsk, Russia, and the improved detectors CMD-3 and SND-2000. The future development of this

⁷ HLMNT use perturbative QCD for the central value of the contribution between 1.8 and 3.7 GeV, but assign the experimental errors from the BES measurements to it.

⁸ The correlation between M_H and $\Delta\alpha_{\text{had}}(M_Z^2)$ reduces to -17% when using the result (15) in the global fit.

field also relies on a more accurate muon $g - 2$ measurement, and on progress in the evaluation of the light-by-light scattering contribution.

I am grateful to the fruitful collaboration with my colleagues and friends Michel Davier, Bogdan Malaescu and Zhiqing Zhang. Mar-

tin Goebel from the Gfitter group is warmly thanked for performing the electroweak fit and producing Fig. 8 of these proceedings. I am indebted to George Lafferty and the helping hands at the University of Manchester who managed to organise a very interesting and pleasant workshop, and who so thoughtfully provided umbrellas against boisterous rain storms.

-
- [1] A. Czarnecki and W.J. Marciano, Phys. Rev. D 64, 013014 (2001).
 - [2] M. Davier and W.J. Marciano, Ann. Rev. Nucl. and Part. Sci. 54, 115 (2004).
 - [3] J. Miller, E. de Rafael and B. Lee Roberts, Rep. Progr. Phys. 70, 75 (2007).
 - [4] F. Jegerlehner and A. Nyffeler, Phys. Reports 477, 1 (2009).
 - [5] P.J. Mohr, B.N. Taylor and D.B. Newell (CODATA Group), Rev. Mod. Phys. 80, 633 (2008).
 - [6] G.W. Bennett *et al.*, Phys. Rev. Lett. 89, 101804 (2002), Erratum *ibid.* Phys. Rev. Lett. 89, 129903 (2002); G.W. Bennett *et al.*, Phys. Rev. Lett. 92, 161802 (2004); G.W. Bennett *et al.*, Phys. Rev. D 73, 072003 (2006).
 - [7] A. Hoecker and W. Marciano, “The Muon Anomalous Magnetic Moment”, in: Particle Data Group (K. Nakamura *et al.*), J. Phys. G 37, 075021 (2010).
 - [8] J. Bailey *et al.*, Nucl. Phys. B 150, 1 (1979).
 - [9] T. Kinoshita and M. Nio, Phys. Rev. D 73, 013003 (2006); T. Aoyama, M. Hayakawa, T. Kinoshita and M. Nio, Phys. Rev. Lett. 99, 110406 (2007); T. Kinoshita and M. Nio, Phys. Rev. D 70, 113001 (2004); T. Kinoshita, Nucl. Phys. B 144, 206 (2005) (Proc. Suppl.); T. Kinoshita and M. Nio, Phys. Rev. D 73, 053007 (2006); A.L. Kataev, arXiv:hep-ph/0602098 (2006); M. Passera, J. Phys. G: Nucl Part. Phys. 31, 75 (2005).
 - [10] G. Gabrielse *et al.*, Phys. Rev. Lett. 97, 030802 (2006), Erratum *ibid.* Phys. Rev. Lett. 99, 039902 (2007); D. Hanneke, S. Fogwell and G. Gabrielse, Phys. Rev. Lett. 100, 120801 (2008).
 - [11] R. Jackiw and S. Weinberg, Phys. Rev. D 5, 2396 (1972); G. Altarelli *et al.*, Phys. Lett. B 40, 415 (1972); I. Bars and M. Yoshimura, Phys. Rev. D 6, 374 (1972); K. Fujikawa, B.W. Lee and A.I. Sanda, Phys. Rev. D 6, 2923 (1972).
 - [12] A. Czarnecki *et al.*, Phys. Rev. D 67, 073006 (2003); M. Knecht, S. Peris, M. Perrottet, E. de Rafael, JHEP 0211, 003 (2002); S. Heinemeyer, D. Stockinger and G. Weiglein, Nucl. Phys. B 699, 103 (2004); T. Gribov and A. Czarnecki, Phys. Rev. D 72, 053016 (2005); A. Czarnecki, B. Krause and W.J. Marciano, Phys. Rev. Lett. 76, 3267 (1996); A. Czarnecki, B. Krause and W.J. Marciano, Phys. Rev. D 52, 2619, (1995); S. Peris, M. Perrottet and E. de Rafael, Phys. Lett. B 355, 523 (1995); T. Kukhto *et al.*, Nucl. Phys. B 371, 567 (1992).
 - [13] M. Knecht, S. Peris, M. Perrottet, E. de Rafael, JHEP 0211, 003 (2002).
 - [14] A. Nyffeler, Phys. Rev. D 79, 073012 (2009).
 - [15] G. Degrandi and G.F. Giudice, Phys. Rev. D 58, 053007 (1998).
 - [16] C. Bouchiat and L. Michel, J. Phys. Radium 22, 121 (1961); M. Gourdin and E. de Rafael, Nucl. Phys. B 10, 667 (1969).
 - [17] S.J. Brodsky and E. de Rafael, Phys. Rev. 168, 1620 (1968).
 - [18] M. Davier, A. Hoecker, B. Malaescu, Z. Zhang, arXiv:1010.4180 (2010).
 - [19] KLOE Collaboration (F. Ambrosino *et al.*), arXiv:1006.5313 (2010).
 - [20] KLOE Collaboration (F. Ambrosino *et al.*), Phys. Lett. B 670, 285 (2009).
 - [21] BABAR Collaboration (B. Aubert *et al.*), Phys. Rev. Lett. 103, 231801 (2009).
 - [22] M. Davier *et al.*, Eur. Phys. J. C66, 127 (2010).
 - [23] CMD2 Collaboration (R.R. Akhmetshin *et al.*), Phys. Lett. B 578, 285 (2004).
 - [24] CMD2 Collaboration (V. M. Aulchenko *et al.*), JETP Lett. 82, 743 (2005); CMD2 Collaboration (R. R. Akhmetshin *et al.*), JETP Lett. 84, 413 (2006); CMD2 Collaboration (R.R. Akhmetshin *et al.*), Phys. Lett. B 648, 28 (2007).
 - [25] SND Collaboration (M. N. Achasov *et al.*), JETP Lett. 103, 380 (2006).
 - [26] M. Davier, A. Hoecker, B. Malaescu, C.Z. Yuan, and Z. Zhang, Eur. Phys. J. C66, 1 (2010).
 - [27] BABAR Collaboration (B. Aubert *et al.*), Phys. Rev. D 71, 052001 (2005).
 - [28] V.P. Druzhinin, “Study of e^+e^- annihilation at low energies”, Presented at 23rd International Symposium on Lepton-Photon Interactions at High Energy (LP07), Daegu, Korea, 13-18 Aug 2007, published in Daegu 2007, Lepton and photon interactions at high energies 134, arXiv:0710.3455.
 - [29] BABAR Collaboration (B. Aubert *et al.*), Phys. Rev. D 76, 092005 (2007), Erratum *ibid.* Phys. Rev. D 77, 119902 (2008).
 - [30] BABAR Collaboration (B. Aubert *et al.*), Phys. Rev. D 73, 052003 (2006).
 - [31] BABAR Collaboration (B. Aubert *et al.*), Phys. Rev. D 77, 092002 (2008).
 - [32] BABAR Collaboration (B. Aubert *et al.*), Phys. Rev. D 76, 012008 (2007).
 - [33] M. Davier, S. Eidelman, A. Hoecker, and Z. Zhang, Eur. Phys. J. C 27, 497 (2003).
 - [34] M. Davier, S. Eidelman, A. Hoecker, and Z. Zhang, Eur. Phys. J. C 31, 503 (2003).
 - [35] A. Pais, Ann. Phys. 9, 548 (1960).
 - [36] Particle Data Group (K. Nakamura *et al.*), J. Phys. G 37, 075021 (2010).
 - [37] P. Baikov, K.G. Chetyrkin, and J.H. Kühn, Phys. Rev. Lett. 101, 012002 (2008).
 - [38] K.G. Chetyrkin, J.H. Kühn and M. Steinhauser, Nucl. Phys. B 482, 213 (1996).
 - [39] M. Davier and A. Hoecker, Phys. Lett. B 419, 419 (1998).
 - [40] H. Flaecher, M. Goebel, J. Haller, A. Hoecker, K. Moening, and J. Stelzer, Eur. Phys. J. C60, 543 (2009); up-

- dated results taken from: <http://cern.ch/gfitter>.
- [41] F. Le Diberder and A. Pich, Phys. Lett. B 286, 147 (1992).
 - [42] BES Collaboration (J.Z. Bai *et al.*), Phys. Rev. Lett. 84, 594 (2000); Phys. Rev. Lett. 88, 101802 (2002); BES Collaboration (M. Ablikim *et al.*), Phys. Lett. B 641, 145 (2006); Phys. Lett. B 677, 239 (2009).
 - [43] T. Teubner, Talk given at Tau 2010 Workshop, Manchester, UK, 13–17 Sep 2010.
 - [44] K. Hagiwara, A.D. Martin, D. Nomura, and T. Teubner Phys. Lett. B 649, 173 (2007).
 - [45] F. Jegerlehner and A. Nyffeler, Phys. Rept. 477, 1 (2009).
 - [46] J. Prades, E. de Rafael, and A. Vainshtein, UG-FT-242-08, CAFPE-112-08, CPT-P092-2008, FTPI-MINN-08-41, UMN-TH-2723-08, arXiv:0901.0306 (2009).
 - [47] R. Alemany, M. Davier and A. Hoecker, Eur. Phys. J. C 2, 123 (1998).
 - [48] ALEPH Collaboration (S. Schael *et al.*), Phys. Rep. 421, 191 (2005).
 - [49] Belle Collaboration (M. Fujikawa *et al.*), Phys. Rev. D 78, 072006 (2008).
 - [50] CLEO Collaboration (S. Anderson *et al.*), Phys. Rev. D 61, 112002 (2000).
 - [51] OPAL Collaboration (K. Ackerstaff *et al.*), Eur. Phys. J. C 7, 571 (1999).
 - [52] M. Steinhauser, Phys. Lett. B 429, 158 (1998).